1. **Final Report DOE Award # DE-FG02-05ER46218, Texas Tech University**

2. **"Cyclic Macromolecules: Dynamics and Nonlinear Rheology"**

PI: Gregory B. McKenna
Co-PIs: Robert H. Grubbs, Julia A. Kornfield

3. **Report of April 25, 2012 for the period August 1, 2008 – March 31, 2012**

4. **Accomplishments:**

Introduction: The work described in the present report had the original goal to produce large, entangled, ring polymers that were uncontaminated by linear chains and to characterize by rheological methods the dynamics of these rings. While the work fell short of this specific goal, the outcomes of the research performed under support from this grant provided novel macromolecular synthesis methods, new separation methods for ring and linear chains, and novel rheological data on bottle brush polymers, wedge polymers and dendron-based ring molecules. The grant funded a total of 8 archival manuscripts and one patent, all of which are attached to the present report. In the following paragraphs we highlight the major accomplishments.

Polymer Synthesis

Cyclic polymer topologies remain a synthetic challenge for polymer chemistry, and a region of untapped potential for material engineering. The cyclic macromolecule synthesis related to the present grant was based on a robust platform for cyclic polymer synthesis that had several perceived advantages.[1,2] These derive from the cyclic nature of all monomers, catalysts and intermediates that participate, leading to a ring-expansion metathesis polymerization (REMP). The technology utilizes ruthenium-based olefin metathesis catalysts with bidentate ligands bearing N-heterocyclic carbene (NHC) and alkylidene moieties that are based on commercially available ruthenium catalysts (Figure 1).Two series of REMP catalysts were synthesized and characterized.[3] The first class contains N-mesityl, N-alkyl imidazol-2-ylidene ligands (denoted **UC-#**; the number indicates the length of the alkylidene chain), while the second class contains the dihydro analogs (**SC-#**). The alkylidene-linked chains are varied from four to seven carbons atoms long (Figure 2).

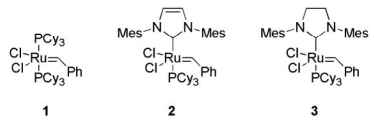

Figure 1. Commercially available ruthenium-based olefin metathesis catalysts

The polymerization kinetics for these catalysts were also investigated, with the aim to determine the factors that influence catalyst activity and molecular weight control (Figure 3).[4] The model that we have developed involves four steps (Figure 3, depicted with a generic REMP catalyst and cyclooctene monomer). As with all living polymerizations, the process contains an initiation step and a propagation step (controlled by rate constants k_i and k_p, respectively). In an initiation kinetics study, the relative observed initiation rates were found to fall in the order SC-**5**>**3**>**UC-5**>**SC-6**>**UC-6**. In general, it appears that linker length is the dominant variable in initiation, where the five-carbon linker promotes faster initiation than the six-carbon linker. The propagation rates were found to fall in the order **SC-6**>**UC-7**>**SC-5**>>**UC-6**>**UC-5**>>**UC-4**. Here, the electronic characteristics of the NHC ligand

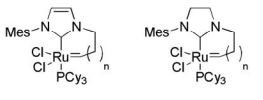

UC-4, n=2
UC-5, n=3
UC-6, n=4
UC-7, n=5

SC-5, n=3
SC-6, n=4

Figure 2. Cyclic ruthenium catalysts for ring-expansion metathesis polymerization (REMP)

have a large influence with the saturated **SC** catalysts outperforming the corresponding **UC** analogs. In order to generate the desired cyclic polymer, the catalyst-containing macrocycle can undergo an intramolecular reaction between the proximal olefin and the alkylidene to extrude cyclic polycyclooctene (cPCOE) and release the original catalyst (k_r). Catalyst release can also occur by intramolecular chain transfer, where olefin metathesis occurs between a distal olefin and the alkylidene, generating a ruthenium-containing macrocycle and an all-carbon macrocycle (k_t). At low conversion, the relative rates of propagation and catalyst release were found to control molecular weight, whereas at high conversion, the rates of intramolecular and intermolecular chain transfer (k_{-t}) were found to become significant and dominate the molecular weight control. In the case of **UC-5** and **SC-5**, catalyst release is fast compared to propagation and the molecular weight remains low. At high conversion, the molecular weight rapidly increases, likely due to intermolecular chain transfer. For **UC-6** and **SC-6**, the opposite is true. Propagation is faster than catalyst release, leading to large molecular weights at low conversion. The molecular weight is eroded at high conversions of monomer, as intramolecular chain transfer becomes the controlling factor.

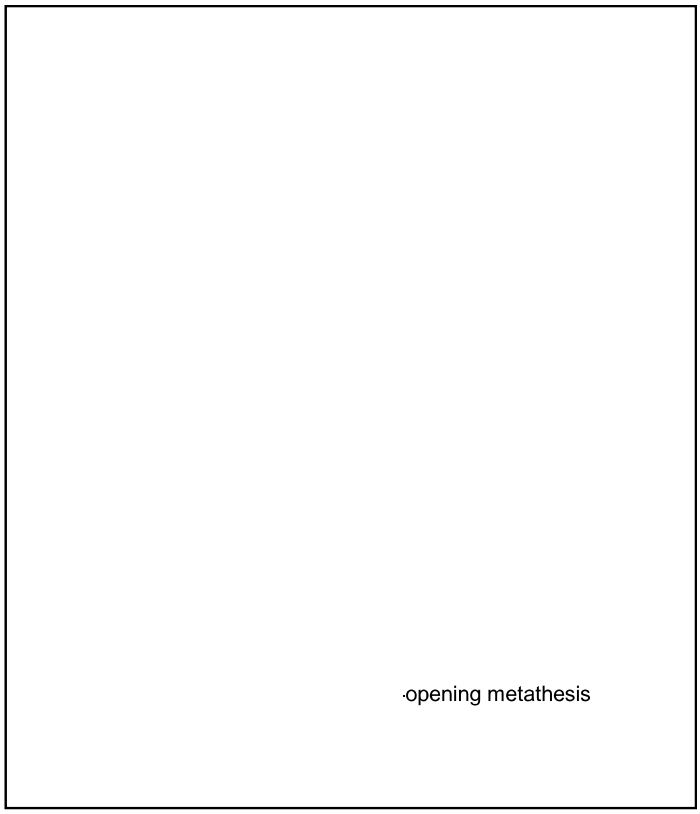

Numerous physical, spectroscopic and microscopic techniques were employed to verify the cyclic nature of REMP products. Our initial report demonstrated there are significant differences between cyclic and linear PCOE in their elution volumes, intrinsic viscosities, hydrodynamic radii and calorimetric properties. Further analysis employed melt-state ^{13}C NMR. This method was chosen because recently developed methods offer higher sensitivity that typical ^{1}H solution-state NMR, especially in the field of polymer chemistry. The spectra for L-PCOE clearly show small additional peaks in the alkyl and olefinic regions that correspond to the end groups of the linear polymer (Figure 4, A and B). For comparison, a cyclic sample was synthesized with **UC-6,** yielded a polymer with M_w=114 kDa and DP=1040 (Figure 4, C and D). The sample clearly lacks end groups, indicating a cyclic topology. Considering the known sensitivity of the technique, we estimate

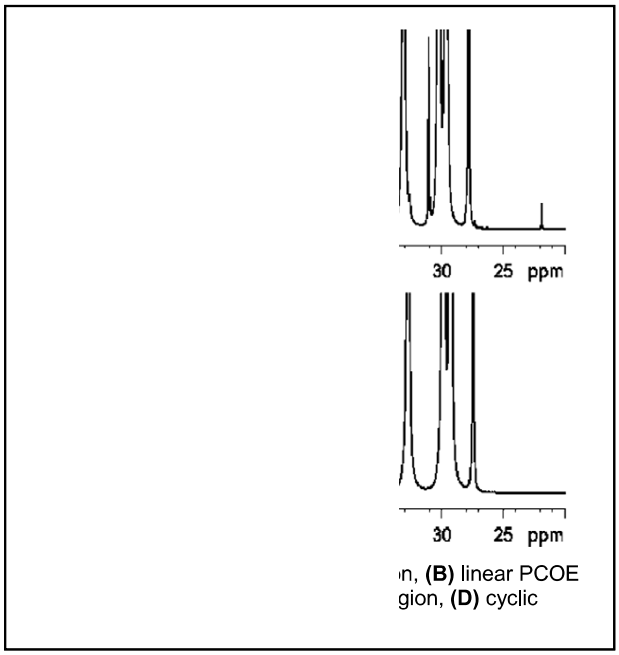

ın, **(B)** linear PCOE
gion, **(D)** cyclic

that the purity of the C-PCOE to be at least 90%. However, this level of purity was found to be insufficient for the characterization of cyclic molecules.

With a good understanding of REMP kinetics and the apparent cyclicity of its polymer products, we moved to the next stage of our collaborative project: a study of the fundamental materials properties of cyclic polymers. Owing to the lack of reliable methods for cyclic polymer synthesis, it has been extremely difficult to effectively evaluate their rheological properties and dynamics. Despite their success, the catalysts developed thus far do not provide pure cyclic polymers, owing to catalyst and monomer degradation. The nature of the impurities precludes them from being removed by traditional methods such as fractionation or column chromatography. Therefore, we have undertaken the design and refinement of a novel method for the purification of cyclic polymers., which we now discuss.

Cyclic and Linear Chain Separation: The major topological difference between linear and cyclic polymers is the existence or absence of end groups, respectively. We sought to exploit this difference with rotaxanation: the threading of a linear molecule through a macrocycle (Figure 6). The Grubbs group has previously disclosed that specially designed ammonium-based polymers will undergo rotaxanation with 24-crown-8 if they possess linear topology (**L-PA** to **T-PA**), but cyclic polymers (**C-PA)** will not.[5]

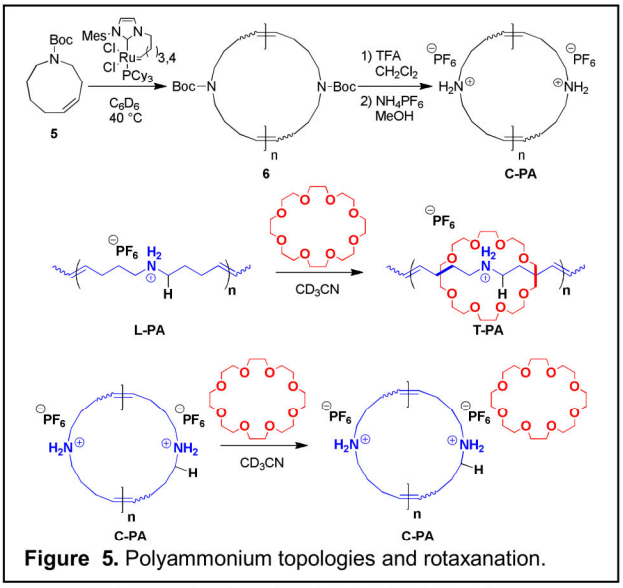

Figure 5. Polyammonium topologies and rotaxanation.

Initial results have shown that we can use rotaxanation to assess the amount of **L-PA** contained within a **C-PA** sample. In these experiments, **C-PA** samples were prepared with various catalyst types and loadings, then treated with 24-crown-8 (Table 1). The ratio of **C-PA** to **L-PA** was measured by ^{1}H NMR. Much of the **L-PA** is believed to arise from olefin migration by Ru-hydride species and subsequent ring scission by hydrolysis. The evidence for this comes from the inverse relation between reaction time (and thus catalyst degradation to Ru-hydride species) and **C-PA/L-PA** ratio. In order to solve the problem of olefin migration, we added benzoquinone to the reaction mixture because it is known to remove Ru-hydride species. As expected, the **C-PA/L-PA** ratio increased (Table 2). The beauty of these monomers is that they allow a careful analysis and purification through threading, however, they are the poorest performing monomers and appear to produce the highest levels of linear contaminates. Further cyclic polymer synthesis will take these findings into account.

Table 1. REMP of **5** and Threading Experiments with **C-PA**

Entry	Catalyst	$[1]_0$ (M)	$[1/C]_0$	Time (h)	M_w (kDa)[b]	PDI	Cyc/Lin[c]
1	**UC-5**	2.0	250	23	485	1.21	80/20
2[d]	**UC-5**	2.0	250	23+24	481	1.24	61/39
3	**UC-5**	2.0	500	47	502	1.23	64/36
4	**UC-5**	2.0	1000	47	633	1.20	70/30
5	**UC-5**	1.5	250	34	412	1.25	67/33
6	**UC-5**	1.0	250	34	393	1.25	66/34
7	**UC-6**	2.0	250	16	237	1.28	45/55
8	**SC-5**	2	250	8	202	1.30	52/48

[a]Reaction Conditions: 40 °C in dry C_6D_6 under N_2 atmosphere. [b]Molecular weight data obtained for polycarbamates**2** via GPC with multiangle laser light scattering. [c]Cyclic/linear ratios determined by ^{1}H NMR spectroscopy in the presence of **24C8**, as described in the text. [d]Reaction mixture maintained at 40 °C for 24 h after monomer conversion was >95% as determined by ^{1}H NMR spectroscopy.

In addition to its applicability as an analytical method, we believe that rotaxanation can be used as a purification tool. We propose two ways that the linear pseudorotaxanes may be removed. Firstly, the **T-PA** and **C-PA** are expected to have

Table 2. Data for REMP of **1** in the presence of BQ and threading experiments of the resulting **C-PA**.[a]

Entry	Catalyst	M_w (kDa)[b]	PDI	Cyc/Lin[c]
1	**UC-5**	354	1.16	87/13
2	**SC-5**	274	1.21	95/5

[a]Reaction Conditions: $[\mathbf{1}]_0$ = 2.0 M, $[\mathbf{1}/C]_0$= 250, $[\mathbf{BQ}/C]_0$ = 10, 40 °C in dry C_6D_6 under N_2 atmosphere. [b]Molecular weight data obtained for polycarbamates**2** via GPC with multiangle laser light scattering. [c]Cyclic/linear ratios determined by ^{1}H NMR spectroscopy in the presence of **24C8**, as described in the text.

different solubility profiles, due to the ability of the crown ether to mask the polyionic nature of the polymer. Initial results have shown that the polyionic nature of **C-PA** limits its solubility in less polar solvents such as benzene or toluene, whereas **T-PA** shows much greater solubility. Initial attempts at selective precipitation of the **C-PA** have had some success. Current work is focused on optimization of precipitation conditions in order to achieve complete removal of the **T-PA** (Figure 6).

Should suitable precipitation conditions not be found, we have also attempted to separate **C-PA** and **T-PA** with a resin-bound crown ether. Dibenzo-24-crown-8 (DB24C8) is an analog of 24-crown-8 that also participates in rotaxanation, and has the added benefit of modifiable positions its aryl rings. We envision a functionalized DB24C8 that is attached to crosslinked polymer resin beads. A solution of **C-PA** and **T-PA** will be treated with the resin-bound DB24C8. Rotaxanation of **T-PA** should bind all the linear contaminants to the beads. Simple filtration of the beads should leave a solution of pure **C-PA** (Figure 6).

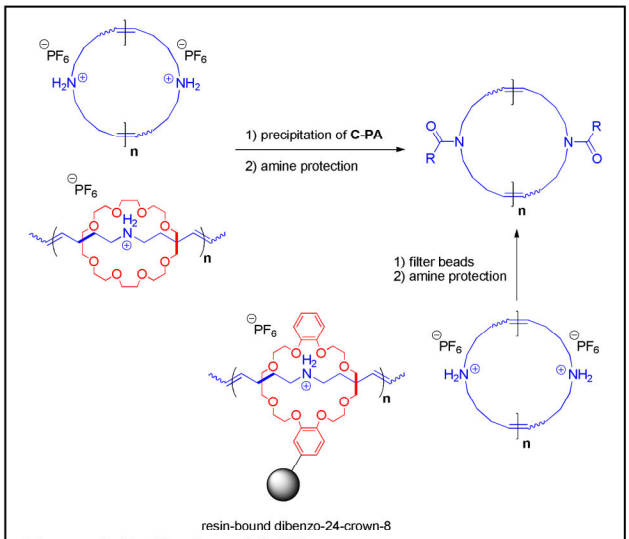

Figure 6. Purification of **C-PA**

Although these methods were used, the ring purity achieved during the present work was never sufficient to give samples that were completely free (>99%) of linear chains. The rheological measurements on these samples are not presented here simply because they showed the presence of contamination by linear chains and inconsistencies in results due to varying amount of contamination. It is recommended that future work on these macrocycles continue with the REMP synthesis and the rotaxanation/filtration method of molecular separations. It is a highly promising technique and suggests high purification capability in specialized applications, such as those demanded in ring macromolecule synthesis.

Because of the difficulties in separations just described, the group also examined other routes to ring synthesis and worked with other molecular architectures. The synthesis methods are based on macromonomer approaches[6] combined with ROMP. This approach to making model bottle-brush molecules is described first followed by discussion of wedge polymers and dendronized rings.

Macromonomer Synthesis of Brush Polymers: The synthesis of high molecular weight brush polymers with good control over side chain lengths, side chain density and backbone lengths is extremely challenging. Of the three current methods to make these molecules (grafting from, grafting onto and grafting through), only the “grafting through” method, which is also called the macromonomer (MM) approach, guarantees complete grafting of the polymer.[6] Still, the MM approach does not always provide good control over the main chain length and the PDI of the polymer.[7] One such MM-based method to make brush polymers is by ring-opening metathesis polymerization (ROMP) of a norbornene-based macromonomer functionalized with the desired side chains (Figure 7). Recently, the group reported on a class of pyridine-

containing ruthenium based catalyst (Figure 8) that has shown both high reactivity and fast initiation for ROMP. Using this catalyst, we were able to synthesize brush polymers with a backbone lengths up to 400 units while still maintaining a narrow polydispersity (PDI < 1.10).[8]

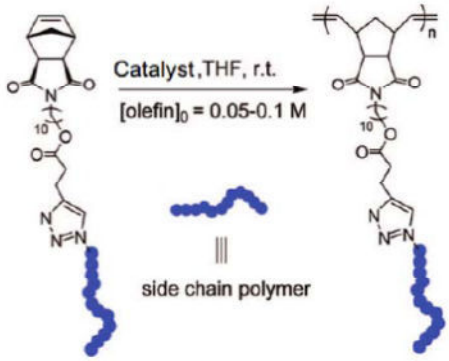

Figure 7. Synthesis of brush polymer using ROMP.

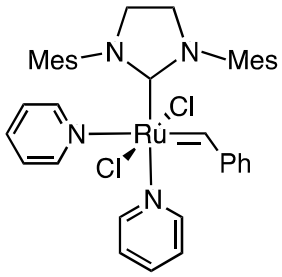

Figure 8. Pyridine containing Ruthenium based catalyst.

We examined several types of brush polymers with different side chains composed of polylactide, polystyrene, and polyacrylates.[9,10] So far, we have employed two different approaches to synthesize the macromonomers. The first method uses a norbornene initiator that is used for the direct polymerization of the macromonomer and the second procedure utilizes click chemistry. In the click approach, the azide end-functionalized side chain polymer is first made and subsequently clicked on a norbornene alkyne. The kinetics of these systems have been studied using varying side chain and backbone lengths.[9,10] Examination of brush copolymers using several different combinations of the above mentioned side chains has also been undertaken.[9] This study has yielded information on the self-assembly of the brush copolymers based on whether it is a random or a block copolymer (Figure 9).

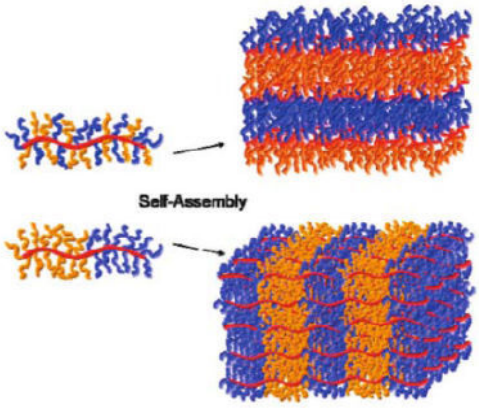

Figure 9. Schematic of self-assembly of brush random copolymer (top) and brush block copolymer (bottom).

The characterization methods used include ^{1}H NMR and gel permeation chromatography (GPC) to analyze the size of the macromonomer, and the subsequent brush polymer has been characterized using GPC and AFM. The AFM images (Figure 10) depict the worm-like structures of the brush polymers and accompanied by the GPC results have provided a way to approximate how stretched the backbone is. The brush copolymers were also analyzed using small angle X-ray scattering (SAXS). This method provided a means to look at the size of the domains formed by the different side chains and consequently determine how the brush copolymers self-assemble as previously mentioned (Figure 10).[10] Subsequently, we detail results from the rheological characterization of one series of model bottle-brush polymers.

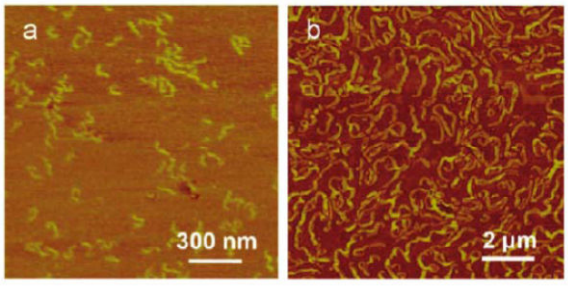

Figure 10. AFM images of (a) polylactide brush polymer and (b) brush block copolymer of polylactide and poly n-butyl acrylate.

Macromonomer/ROMP Polymer Syntheses: Clearly, monomer structure can have profound influences on polymer topology, stereochemistry and materials properties. Versatile monomer constructs are valuable tools for the study of polymer behavior, as incremental changes in pendant functional groups can manifest themselves in macromolecular properties. To further investigate such effects, we designed and synthesized a wedge-shaped monomer (**WM**) that can both influence polymer backbone topology as well as side-group interactions. The synthesis is straightforward (Figure 11) and allows for the incorporation many different functional groups. The first step is the alkylation of methyl gallate to compound **7**. The depicted wedge monomer acquires dodecyl groups from this step, but many electrophiles are suitable and will allow us to easily produce an array of monomers. The remaining two steps are saponification to **8** and a Steglich esterification with norbornene **9** to obtain **WM**. All steps are accomplished in good to excellent yield. Ring-opening metathesis polymerization (ROMP) of **WM** to **PW** is initiated with ruthenium-based catalyst **10**.

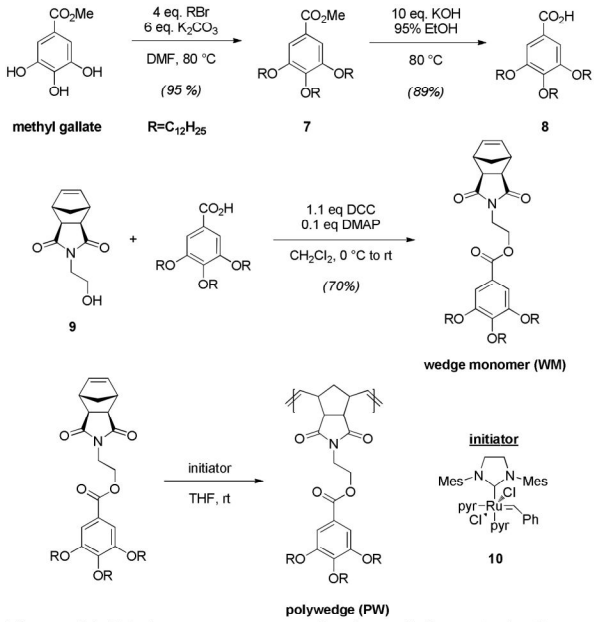

Figure 11. Wedge monomer synthesis and characterization

Polymers are synthesized on gram-scale with good molecular weight control and low PDIs. Rheological characterization of a series of wedge polymers is described in a later section.

Frechet and coworkers have shown that polymers of dendritic macromonomers such as **4** can be synthesized[11] and visualized using atomic force microscopy (AFM). To this end, macromonomer **4** was treated with **UC-6** to obtain a cyclic polymer **C-P4** (M_w=3790 kDa, DP=4210, PDI=1.18). Polymer **C-P4** was then applied to freshly-cleaved mica and examined by AFM (Figure 12). It is evident from the obtained images that **C-P4** forms toroidal structures on the mica surface. The line scans also indicated a uniform structure between individual polymer chains. Linear analogs were prepared and demonstrated no toroidal features when visualized by AFM.[11] Rheological behavior of a set of synthesized dendron-based rings and linear chains is presented in a later section.

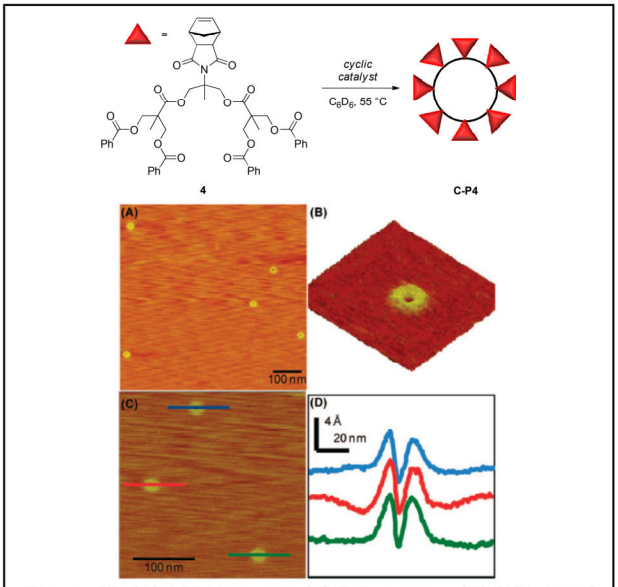

Figure 12. (A) AFM images of **C-P4** on mina. **(B)** 3-D plot of toroidal feature. **(C)** Three toroids from image A. **(D)** Line scans of toroids in image C.

Rheological Characterization of Model Polymers: Three classes of model polymers were synthesized and the dynamic rheology of the systems was measured. These were, first, a series of bottle-brush polymers having different chain length (degree of polymerization) and different side chain length. Second, we examined a set of wedge-type polymers and, finally, we investigated the response of the dendron-based macrocycles.

Bottle Brush Polymers: The polynorbornene-g- poly-(D, L)-lactide brush polymers used in the present study[10] were synthesized by previously described ring-opening metathesis polymerization (ROMP) of norbornenyl macromonomers (MMs) (Figure 13)[9,10]. The molecular weights of the MMs and the brush polymers were controlled by the ratio of the monomer (or MM) to the initiator. The polylactide side chains had molecular weights from 1.4 kg/mol to 8.7 kg/mol and the backbone DPs were 200, 400 or 800. Table 3 shows the molecular characteristics of the molecules.

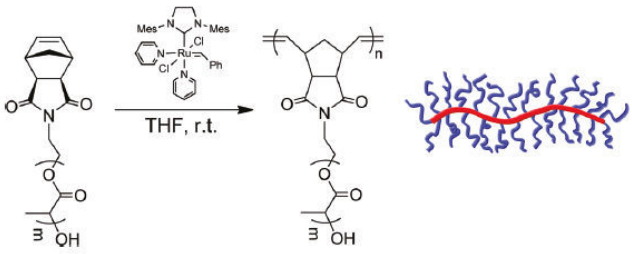

Figure 13. Scheme of the synthesis of polynorbornene-g-polylactide brush polymers and schematic of the molecule.

Table 3. Bottle brush polymer molecular characteristics.

sample number	M_{br}[a] (kDa)	DP[b]	M_w[c] (kDa)	PDI[d]	φ_{br}[e]
P(PLA1.4)-200	1.4	200	350	1.01	0.893
P(PLA1.4)-400		400	680	1.02	0.898
P(PLA1.4)-800		800	1510	1.04	0.900
P(PLA4.4)-200	4.4	200	840	1.02	0.951
P(PLA4.4)-400		400	2240	1.02	0.956
P(PLA4.4)-800		800	4880	1.03	0.958
P(PLA8.7)-200	8.7	200	1600	1.02	0.970
P(PLA8.7)-400		400	3660	1.08	0.975
P(PLA8.7)-800		800	6050	1.07	0.977

[a] M_{br} is the molecular weight of the side chains. [b] DP is the degree of polymerization of the backbone. [c] M_w is the molecular weight of the brush polymer determined by GPC–MALLS in THF. [d] Polydispersity index (PDI) of the brush polymer. [e] φ_{br} is the volume fraction of the side chain estimated by the group contribution method.[31]

Dynamic Response of the Brush Polymers

Figure 15 presents dynamic master curves at 80 °C for the brush polymers having a DP of 200 and different side chain molecular weights over the full range from the glassy plateau to the terminal flow region. The curves are vertically shifted to separate the data for each different side chain length. The figure show clearly that from the glassy state to the terminal flow region, several different relaxation behaviors appear in sequence. In the following sections, we plot the dynamic master curves for all of the polymers in different ways and compare the influence of side chain length and backbone DP to the sequential relaxation behaviors

Dilute solution properties

The intrinsic viscosity ([η]) and molecular weight for these brush polymers with different side chain and backbone lengths were measured using GPC coupled with a light scattering detector and a viscometer. As shown in Figure 14, for the three groups of brush samples with fixed side chain molecular weight but increasing DP, the slope of log([η]) vs log(Mw) decreases from 0.67 to 0.55 as the side chain molecular weight increases.

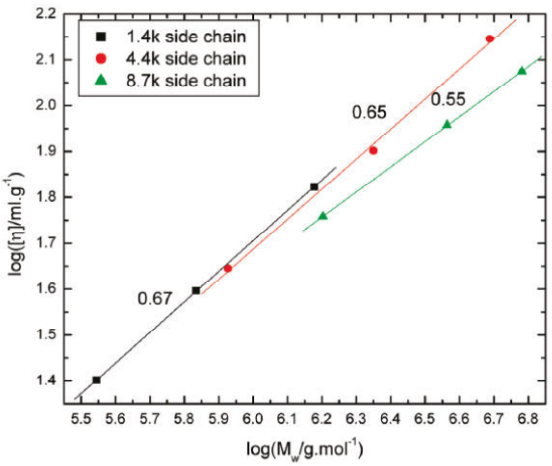

Figure 14. Intrinsic viscosity versus molecular weight for brush polymers. with fixed side chain molecular weight but increasing DP (in THF at room temperature ≈ 25 °C).

of these densely branched brush polymers. In the terminal zone, most of the densely branched brush samples seem to behave in a Rouse-like manner. There is little evidence of entanglement. For linear polymer materials increasing the backbone length leads to a longer relaxation time and the terminal flow region will move to a lower frequency[12]. On the other hand, when we compare brush samples with the same backbone DP, the terminal relaxation time not only depends on the DP of the polymer, but also increases with increasing side chain molecular weight. Similar phenomena have been observed for other brush or comb polymers with fixed backbone length and the influence of the side chains on the relaxation of the backbone was invoked to explain this phenomenon. For the samples with 4.4k and 8.7 kDa side chains, two rubbery plateau regions were observed in the dynamic master curve and the first plateau from the glassy modulus region at intermediate frequencies becomes more obvious, while the second plateau gradually develops as the DP increases. Such a two plateau region phenomenon is referred to as a double relaxation mechanism which is typical for brush, comb, or star polymers with long side chains[13,14,15,16,17,18,19,20,21,22,23,24].

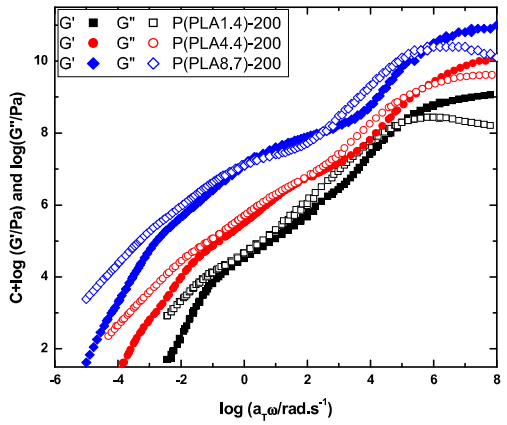

Figure 15. Comparison of the dynamic responses of the brush polymers with fixed DP of 200 and differing side chain lengths, as indicated..

To clarify the attribution of the two plateaus in the dynamic spectrum for the brush polymers with different side chain molecular weight, the dynamic master curves were plotted following the van Gurp-Palmen method[25] by plotting the phase angle (δ) vs the logarithm of the complex modulus |G*|. The van Gurp_Palmen plot is sensitive to the molecular weight and molecular architectures of the materials and provides an excellent tool to estimate the value of the plateau modulus[26]. The van Gurp_Palmen plots for the DP dependence and the side chain molecular weight dependence of several brush samples are shown in Figure 5, parts a and b. Similar to the two plateau phenomenon discussed in relation to the dynamic curves, there are two minima in the phase angle (δ) vs log|G*| plot for most of the brush samples. As shown in Figure 16a, for the first minimum in the phase angle (δ) at higher modulus, the |G*| values and phase angle (δ) values are almost independence of the DP with fixed side chain molecular weight. While in Figure 16b, for fixed backbone DP and increasing side chain molecular weight, the |G*| values at the first minimum are almost fixed but the δ value decreases. In van Gurp-Palmen plots for linear polymers, as the molecular weight increases, the δ value will decrease and the |G*| values do not change[26]. Hence, parts a and b of Figure 16 suggest that the first minimum in the van Gurp-Palmen plot, which corresponds to the first plateau in the dynamic master curve, should be related with the relaxation of the side chains. The plateau modulus of the polylactide is reported to be approximately $5x10^5$ Pa and the entanglement molecular weight is approximately 8.7 kDa[27]. In parts a and b of Figure 16, the corresponding |G*|values for the first plateau is approximately $6.3x10^5$ Pa, which is again near to the plateau modulus value for the polylactide.

Sequential Relaxation

It is expected that branched polymers should relax sequentially. The chain segments should relax first, followed by the side chains, and the whole polymer should be the last to move[13,15,23]. Rheooptical study of a similar densely branched polymer shows relaxation that follows the same

sequence as regular branched polymers[28]. To examine the sequential relaxation behaviors of

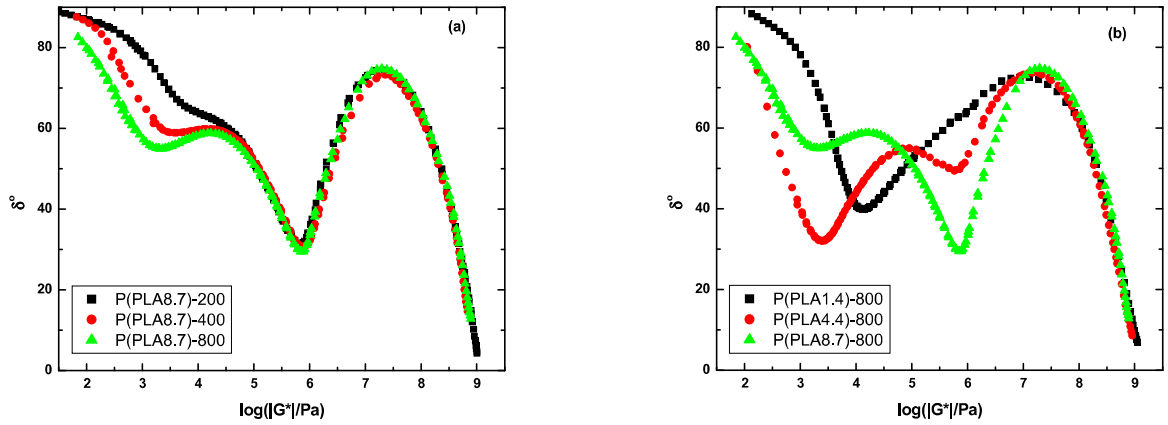

Figure 16. van Gurp-Palmen plot for brush polymers with (a) fixed side chain molecular weight and (b) fixed backbone DP.

the brush polymers, we lot the storage modulus (G0) master curves of brush polymers having the same side chains shifted horizontally to match in the segmental regime. The slight horizontal shifting was applied to compensate for the modest differences in glass transition temperatures among the samples. As shown in Figure 17, the master curves can be divided into three regimes: the segmental regime, the arm regime, and the terminal regime. For the brush polymers with the same side chains, when their glass transition regions are shifted together, the arm regimes overlap with each other very well. The length of the arm regime increases with increasing side chain length. In the terminal region, the curves start to deviate from each other moving to lower frequency as the DP of the backbone increases.

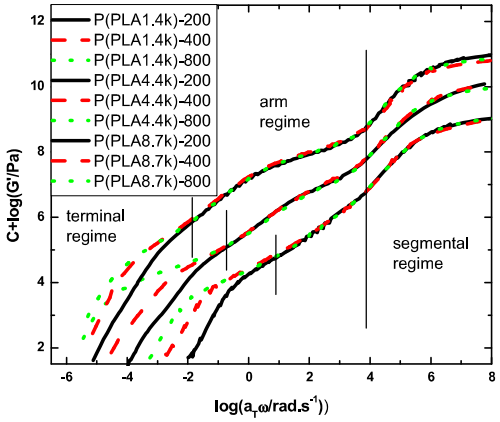

Figure 17. Sequential relaxation of the brush polymers (vertical shift of C = 0, 1, and 2 used to separate the respective the curves).

Segmental Regime The segmental regime covers the glassy and glass transition region of the brush polymers. If one compares the curves in Figure 17 and Figure 18, the side chain length and backbone DP have only minor effects on the glassy moduli (Gg). The glassy modulus value of the brush polymer is around 10^9 Pa which is much higher than that of polynorbornene and is closer to that of linear polylactide[29].

Arm Regime Figure 18 shows an expanded plot of the arm regime for the brush polymers with shifting

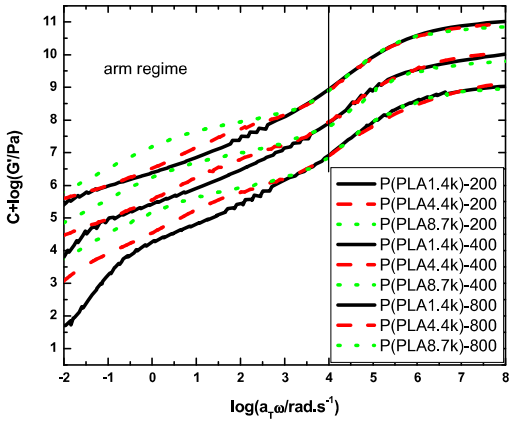

Figure 18. Expanded plot of the arm regime and segmental regime for the brush polymers with fixed DP (vertical shift of C = 0, 1, and 2 used to separate the respective DP curves).

the polymers with the same DP together. By shifting the samples with the same backbone DP together, the influence of arm length on the relaxation behavior of the brush polymer can be readily demonstrated. For each group of samples with the same backbone DP, a clear plateau is seen for samples with the 4.4 kDa and 8.7 kDa side chain. The plateau values are 6.3×10^5 and 6.2×10^5 Pa, which are independent of the arm length and backbone DP. This regime is missing or difficult to detect in the samples with the 1.4 kDa side chain molecular weight. As shown in Figure 18, the plateau found in the relaxation behaviors of the arm regime are affected by both the faster segmental relaxation and the slower terminal relaxation processes. Rather than using the dynamic data of Figure 18, a better resolution of the arm relaxation can be achieved using the retardation spectra ($L(\tau)$) of the different brush polymers and these were calculated. The retardation spectra of the brush polymers with the same 200 backbone DP but different side chain molecular weight are plotted in Figure 19. Horizontal shifting was applied to overlap the glassy regions and eliminate the effects of the differences between the glass transition temperatures. According to Plazek[30,31], in the retardation spectra of entangled polymers, there are usually two peaks with similar heights. The length between the two peak points corresponds to the length of the rubbery plateau. In Figure 19, only one peak is found in all of the retardation spectra. With the increase of the side chain molecular weight, a shoulder plateau region can be seen and this increases in length with increasing side chain molecular weight. If one integrates the retardation spectrum over the relaxation time (τ), the shoulder region in the spectrum corresponds to the side chain relaxation as seen in the relevant dynamic curves. The length of the shoulder region can be estimated as the distance between the glass transition region and the transition region from arm relaxation to the terminal relaxation. If the side chains are entangled, then the length of the shoulder plateau should increase with the 3.4 power of molecular weight.[12] However in Figure 19, the relaxation time only scales approximately as the 2.3 power of the side chain molecular weight, which is consistent with the side chains being unentangled, Rouse-like chains. The unentangled nature and Rouse-like behaviors of side chains are similar to the treatment of the side chains in some current model predictions[13,24,32,33].

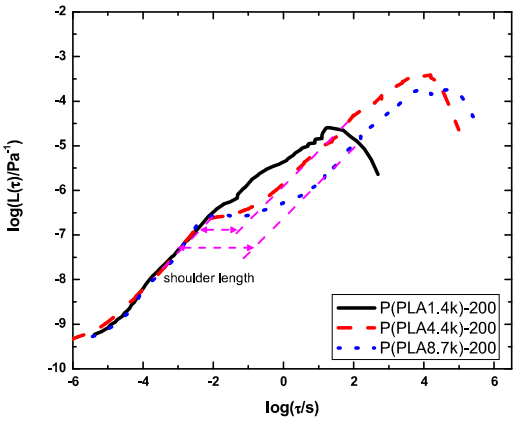

Figure 19. Double logarithmic representation of the retardation spectra from the creep data. ($L(\tau)$) for brush polymers with fixed 200 DP backbone and different side chain molecular

Terminal Regime Figure 20 presents an expanded plot of the terminal regime and shows the relaxation behavior of the backbone. In the plot, a not very obvious plateau in the storage modulus curve can be found for each sample. This plateau corresponds to the second plateau found in the van Gurp-Palmen plot discussed previously. The modulus values for this plateau can be accurately estimated from the van Gurp-Palmen plot (Table 4). In the terminal regime, the whole polymer molecule relaxes. Thus the modulus value should decrease following the same ratio of the increasing DP. If we take the modulus values of the 800DP samples as references and mark them as $G'_{1.4}$, $G'_{4.4}$, and $G'_{8.7}$, respectively, for different side chains, then it is found that the storage modulus values decrease nearly linearly with increasing DP. The plateau shown in Figure 20 looks like a rubbery plateau for the brush polymers. However, for an entangled polymer material, the rubbery plateau modulus should be a constant value and independent of the DP[12]. To further examine this, the steady state recoverable compliance (J_s) values for the brush polymers were estimated from the creep data using the equation, $J(t) =$

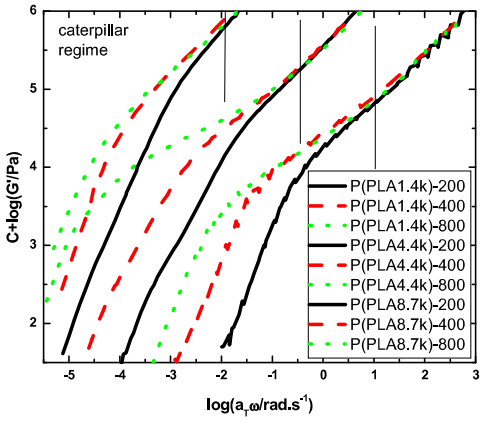

Figure 20. Expanded plot of the terminal regime for the relaxation of the brush polymer with fixed side chains (vertical shift of C = 0, 1, and 2 used to separate the curves).

$J_R(t) + t/\eta$. The J(t) is the shear creep compliance and η is the steady shear viscosity. $J_R(t)$ is the recoverable compliance. According to Plazek[30,31], for not well entangled polymers, the plateau or shoulder observed in the dynamic modulus data is not the rubbery plateau. It simply reflects the molecular orientation and is not the entropy due to the deformation of a chain entanglement network. The storage modulus value that appears to be a rubbery response in unentangled or lightly entangled linear polymers is, rather, the inverse value of the steady state recoverable compliance (J_s). The G'_0J_s is expected to equal 1, and $\log(G'_0)$ is equal to the negative $\log(J_s)$. The value of G'_0 on this lower plateau is readily estimated from the van Gurp-Palmen plot. If it is the rubbery plateau, theoretically it should be twice the reciprocal of the steady state recoverable compliance ($G_N^0 = 2/J_s$)[12] Thus if the plateau associated with the backbone (G'_b) is not the rubbery plateau, then we expect $\log(J_s) = -\log(G'_b)$. The log values of plateau modulus (G'_b) in the terminal regime estimated from the van Gurp-Palmen plot and steady state recoverable compliance (J_s) obtained from the creep experiments are listed in Table 3. As shown in Table 3, the value of G'_bJ_s is generally near to Plazek's prediction of 1 for unentangled polymer chains. Thus, following Plazek, the backbone plateaus found in the dynamic curves reflect the chain orientation for these stiffened polymers and the plateaus observed are not due to entanglements.

Table 4. Estimated backbone plateau modulus (G'_b) and steady state recoverable compliance (J_s) for the brush polymers at 80°C

Polymer	$\log(G'_b)$ [a]	$\log(J_s)$ [b]	G'_bJ_s	G'_b ratio [c]
P(PLA1.4)-200	4.64	-4.55	1.2	$3.3G'_{1.4}$
P(PLA1.4)-400	4.38	-4.26	1.3	$1.8G'_{1.4}$
P(PLA1.4)-800	4.12	-3.96	1.4	$1.0G'_{1.4}$
P(PLA4.4)-200	4.11	-4.08	1.1	$5.2G'_{4.4}$
P(PLA4.4)-400	3.72	-3.62	1.3	$2.1G'_{4.4}$
P(PLA4.4)-800	3.39	-3.24	1.4	$1.0G'_{4.4}$
P(PLA8.7)-200	3.96	-3.94	1.0	$4.6G'_{8.7}$
P(PLA8.7)-400	3.62	-3.24	2.4	$2.1G'_{8.7}$
P(PLA8.7)-800	3.30	-3.07	1.7	$1.0G'_{8.7}$

From the above it is clear that there is no entanglement in either the arm regime or the terminal regime. Then for these brush polymers of very high molecular weight, are they all Rouse chains? We found that for the brush polymers with the same backbone DP, the Js values increase with side chain length. This shows the increasing dilution effect with side chain length. For the brushes with the same side chain molecular weight but different DP, the steady state recoverable compliance (J_s) increases with DP, and the Js value is expected to approach a plateau at higher DP. This seems to be the case for the 1.7 kDa and 8.7 kDa side chain brushes, but is less clear for the 4.4 kDa samples. Such a trend is similar to what is expected for linear chains and is consistent with these brushes being in the transition zone from the Rouse like chain to the fully entangled melt.

There are slight differences between the glass transition temperatures (T_g) of these brush polymers. The zero shear viscosities (η_0) at the same experimental temperature therefore do not correctly reflect the viscosity dependence on molecular weight. We used the WLF equation to correct the viscosity values to the same temperature distance from their corresponding glass transition temperatures. To further clarify the entanglement conditions for the brushes in the melt, the zero shear viscosities (η_0) at Tg+30 ^oC for the three series of samples were determined as a function of weight average molecular weight and it was found that viscosity data follows a power law of approximately 1.7 with M_w, and this is consistent with these brush samples being in the transition zone from the unentangled near linear dependence on M_w toward but not reaching entangled behavior, where the exponent would be 3.4[12].

Macromonomer Systems:

Wedge Polymer: The first macromonomer system that combined ROMP-synthesis was the so-called wedge polymer. Figure 21 shows the structure of this polymer side group on the polynorbornene backbone (see also Figure 11). These can be made at very large DP and good polydispersity control: M_w/M_n=1.09. Table 5 shows the properties of the wedge polymers studied here.

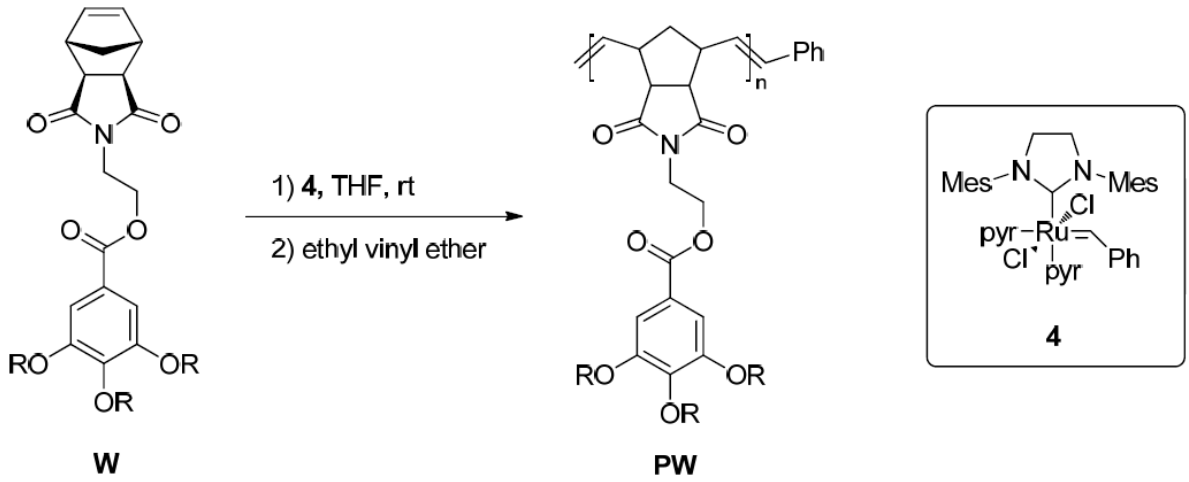

Figure 21. Scheme of the synthesis of the wedge polymers.

Table 5. Wedge polymer molecular weight and characterization data.

Sample number	DP [a]	M_w [b] (kDa)	PDI [c]	φ_{br} [d]	T_g [e] (^oC)
273-1	1001	2815	3.26	0.876	42.8
273-2	699	1164	1.93	0.876	42.2
221A	1406	1347	1.11	0.876	42.9
221B	5314	5713	1.25	0.877	43.4

[a]DP is the degree of polymerization of the macromonomers (MMs); [b] M_w is the molecular weight of the wedge polymer determined by GPC-MALLS in THF; [c] Polydispersity index(PDI) of the wedge polymer; [d]φ_{br} is the volume fraction of the side chain was estimated by the group contribution method[34,35] ;[e]The glass transition temperature (T_g) of the wedge polymer determined from the dynamic temperature ramp curve.

Chain conformation in solution. The radius of gyration (R_g) of the wedge polymer with different backbone DP was measured using GPC coupled with a light scattering detector. As shown in Figure 22, the size of the wedge polymer increases with increasing molecular weight and the slope for the $\log(R_g)$ vs $\log(M_w)$ is 0.75, which indicates that the THF is a good solvent for the wedge polymer at room temperature.

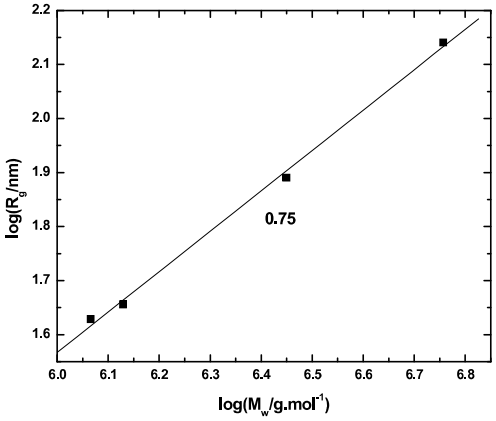

Figure 22. The radius of gyration (R_g) change for wedge polymer with different molecular weight in THF at room temperature (≈25°C).

Dynamic response of the wedge polymers Figure 23 shows the dynamic master curve for the four wedge polymers at a reference temperature of 80°C. Unlike the brush polymers described above, in the dynamic master curves of the wedge polymers, there is only one rubbery plateau with a magnitude of approximately (G_N^0) = 1.3×10^4 Pa, corresponding to an entanglement molecular weight of M_e =2.26×10^5 g/mol. Thus the number of entanglements per chain of the wedge polymers examined in this work is between 4 and 25. In the terminal zone, the relaxation time increases with increasing backbone DP or molecular weight of the wedge polymer.

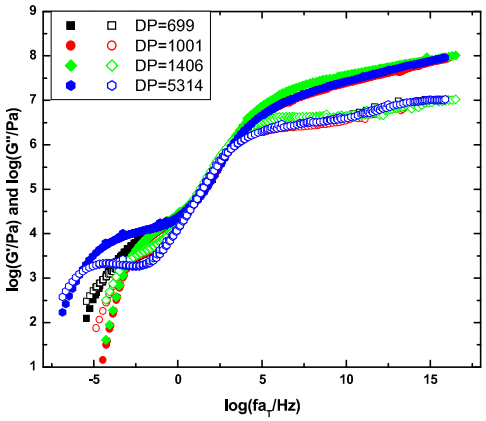

Figure 23. The dynamic master curves for wedge polymers of different backbone DP at a reference temperature of 80°C.

The wedge polymer is a branched polymer with polynorbornene backbone and a unique branch structure. Within the experimental temperature range, the measured glassy modulus of the wedge polymer is near 10^8Pa. Mather et. al.[36] measured the tensile storage modulus (E') and loss modulus (E") of polynorbornene at different temperatures. At the temperature of -20°C, which is the lowest temperature in our experiments, the E' was found to be 8×10^8 Pa. Estimating the shear modulus from the tensile modulus, the storage modulus (G') for linear polynorbornene is then approximately 3×10^8 Pa. Influenced by the bulky side chain structure, the polymer does not densely pack, and the wedge polymer consequently, exhibits a lower glassy modulus than the pure linear polynorbornene.

Figure 24 depicts the shift factors used to construct the dynamic master curves. The shift factors for the four samples are almost the same. The shift factor data at higher temperature can be well fitted by the Williams-Landel-Ferry (WLF)[12,37] equation. Influenced by the experimental thermal history, after the glass transition region the samples are out of equilibrium and the shift factors deviate from the equilibrium line predicted by the WLF fitting.

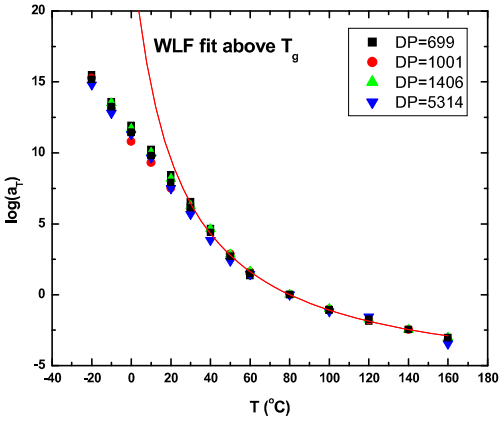

Figure 24. Time-temperature shift factors for wedge polymers of different backbone DP.

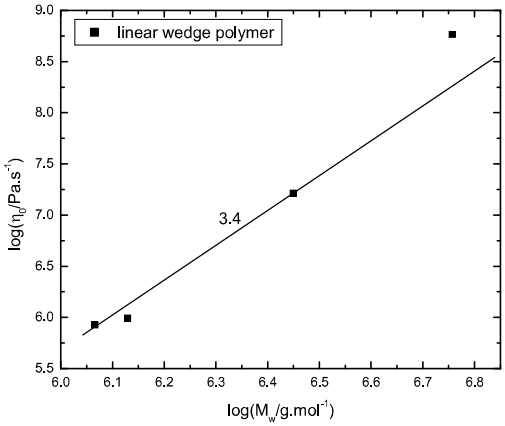

Figure 25. The zero shear viscosity for the wedge polymer vs. molecular weight at the reference temperature of 80°C.

Zero shear viscosity of the wedge polymers Finally, Figure 25 shows the increase of the zero shear rate viscosity for the wedge polymers as a function of molecular weight. The scaling of the viscosity with molecular weight follows a power law typical of entangled linear chains, i.e.,

$$\eta_0 \approx \mathrm{M_w^{3.4}}$$

Conclusions: In conclusion, a series of wedge polymers with bulky side chains and polynorbornene backbone were synthesized via ROMP of poly(macromonomers). Similar to other branched polymers with bulky side chain structure, the plateau modulus of the wedge polymer is low and due to the difficulty of entanglement of such bulky chains. Affected by the bulky side chain structure, the glass transition temperature of the wedge polymer is higher than for the linear polynorbornene, but the wedge polymer shows a much lower glassy modulus with the value around 10^8 Pa.

Dendron-Based Ring Polymers:

Synthesis of dendronized rings Because of the difficulty in synthesis this complex macromonomer, only one dendronized polymer ring was prepared during the course of the present study. The molecular weight of the dendronized polymer ring was 5.658 x 10^6 Da and the polydispersity index PDI=1.16. If estimated from the molecular weight of the macromonomer, the DP is around 4740. To compare the viscoelastic properties of the dendronized macrocyclic polymer, we also needed to prepare the dendronized polymer with linear structure. However, limited by the steric hindrance, the ring structure is more favorable for this kind of macromonomer, which is why it is favorable as a candidate for ring polymer synthesis. With ring opening metathesis polymerization (ROMP), it is difficult to obtain linear dendronized polymers with higher backbone degree of polymerization (DP). Hence, to prepare linear dendronized polymers, ultrasound was used to break the high DP dendronized rings into linear chains. As discussed below, this does not result in exactly comparable linear samples to the original ring because large amounts of the dendron side chains are broken along with the cleavage of the backbone of the polymer rings. Hence, the ultrasound prepared linear chain may not bare the same structure as the dendronized macrocyclic polymer. The only linear

sample prepared by the ultrasonication had a molecular weight of 3.23 x 10^6 Da and the PDI was 1.38 with a corresponding backbone DP of approximately 2230.

Viscoelastic properties of dendronized rings The dynamic master curve of the dendronized polymer ring sample at a reference temperature of 80 °C is shown in Figure 26. The examined temperature range was from 45 °C to 200 °C and was limited at the high end by concerns of sample degradation. Thus in the dynamic master curves, the sample does not quite reach the terminal flow region.

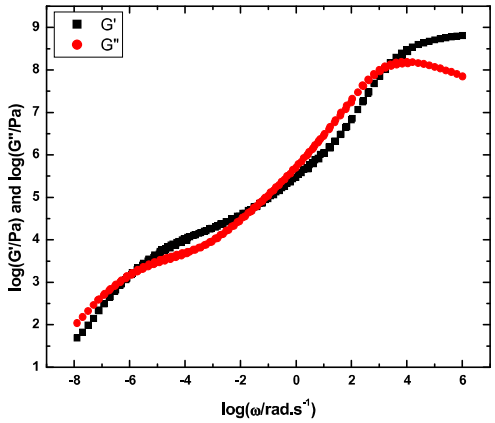

Figure 26. The dynamic master curves of storage (G') and loss (G'') moduli for the dendronized polymer ring sample at a reference temperature of 80 °C.

As shown in Figure 26, the dendronized polymer ring shows a clear glassy plateau with the modulus (G_g) near 10^9 Pa. The rubbery plateau modulus (G_e) is approximately 1.42x10^4 Pa. We also performed a creep experiment at 120°C and this gives the plateau compliance (J_e) of approximately 7.69x10^{-5} Pa^{-1}, which gives a plateau modulus ($G_e=1/J_e$) value of approximately 1.3x10^4 Pa. If the plateau found in the dynamic master curve is the entanglement plateau of the macrocyclic polymer, then the estimated number of entanglements per chain for this macrocyclic polymer would be around 27, which would be greater than the entanglement density of any previous synthetic rings investigated, and significantly greater than the recent results for polystyrene reported by Kapnistos et al[17] which was fewer than 10 even if the entanglement molecular weight of the rings is as small as that for the linear chain, which seems doubtful based on the prior studies from McKenna and co-workers[38,39] and from Roovers and Toporowski[40]. The zero shear viscosity at 120 °C for the ring polymer was found to be 8.85x10^6 Pa.s. The recoverable compliance $J_R(t)$ was estimated from the creep data with the equation[12] $J_R= J(t)-t/\eta_0$ (see Figure 27). Then, the steady state recoverable compliance J_s could be determined from the long-time limiting value. We found from this procedure that J_s = 3x10^{-3} Pa^{-1}, hence J_sG_e for the ring polymer is 39, which is significantly larger than what is expected for linear chains. If this is a true ring polymer, the high value of J_sG_e remains unexplained by theory. However, at this stage of understanding, it is also possible that the dendronized ring is contaminated by linear chains, which would greatly increase the value of J_s, as shown by McKenna and Plazek[39,41] in studies of blends of linear and cyclic polymer. Yet, the AFM images (see Figure 12) do not show linear counterparts to the rings. Furthermore, the very low value of the plateau modulus is also suggestive of difficulty in entanglement and a different chain dynamics for rings vis-à-vis linear polymer chains. This avenue of research should be further pursued.

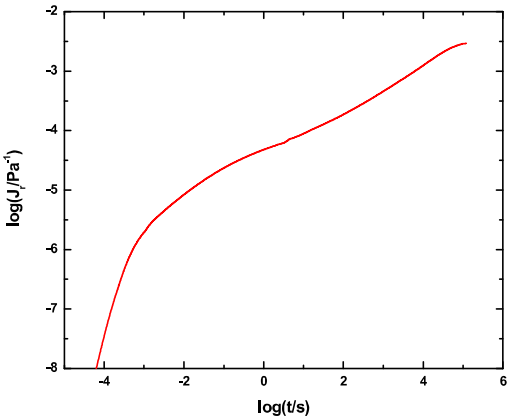

Figure 27. The recoverable compliance of dendronized polymer ring at 120 °C.

From the above, it appears that the dendronized polymer ring shows quite different viscoelastic properties than normal entangled linear polymers. The dendronized polymer ring has a very complex molecular structure. Based on model predictions[17,42,43,44,45], the ring structure should not entangle. But in the present data, we see a clear rubbery plateau. Estimating the volume fraction of the dendronized side chains through group contribution methods[34,35], the volume fraction of the side chain should account for over 75% of the total volume of the cyclic sample. Hence, the side chains should act as solvent to dilute the backbone and lower the plateau modulus and increase the steady state recoverable compliance value[13,15,22,24,46,47].

Summary and Recommendations

The work performed under the present grant, provided novel macromolecular synthesis methods, new separation methods for ring and linear chains, and novel rheological data on bottle brush polymers, wedge polymers and dendron-based ring molecules. The grant funded a total of 8 archival manuscripts and one patent, all of which are attached to the present report.

The outcomes of the work demonstrate the power of ROMP based chemistry to create novel molecular architectures and of rheological methods to characterize those architectures. In fact, the sensitivity of rheological measurements showed that the goal of achieving large macromolecular rings of simple backbone structure remains elusive. However, novel methods of linear chain separation from the rings were developed and novel macromonomer rings were synthesized using ROMP chemistry. It is recommended that the methods developed here be refined and broadened. It is the view of the authors of this report that these methods can eventually achieve large macromolecular rings uncontaminated by linear chains and, consequently, resolve a major outstanding problem in polymer chain dynamics, viz., how do large rings move.

5. Publications in Which DOE Support is Acknowledged

1) Y. Xia, B.D. Olsen, J.A. Kornfield and R.H. Grubbs, "Efficient Synthesis of Narrowly Dispersed Brush Copolymers and Study of Their Assemblies: The Importance of Side Chain Arrangement," J. Am. Chem. Society, **131**, 18525-18432 (2009).
2) Y. Xia, A. J. Boydston and R. H. Grubbs, "Synthesis and Direct Imaging of Ultrahigh Molecular Weight Cyclic Brush Polymers," Agnew. Chem. Int. Ed., **50**, 5882-5885 (2011).
3) Y. Xia, Y. Li, A.O. Burts, M. F. Ottaviani, D.A. Tirrell, J. A. Johnson, N. J. Turro and R.H. Grubbs, "EPR Study of Spin Labeled Brush Polymers in Organic Solvents," J. Am. Chem. Society, **133**, 19953-19959 (2011).
4) C.P. Park, M.M. Van Wingerden, S-Y. Han, D-P. Kim and R. H. Grubbs, "Low Pressure Ethenolysis of Renewable Methyl Oleate in a Microchemical System," Organic Letters, **13**, 2398-2304 (2011).
5) M. Hu, Y. Xia, G. B. McKenna, J. A. Kornfield and R. H. Grubbs, "Linear Rheological Response of a Series of Densely Branched Brush Polymers," Macromolecules, **44**, 6935-6943 (2011).
6) A.J. Boydston, R.H. Grubbs, C. Daeffler and N. Momcilovic, *On-Demand Photoinitiated Polymerization,* U.S. Patent application # *20120035293, Feb. 9, 2012.*
7) A. J. Boydston, T. W. Holcombe, D. A. Unruh, J. M. J. Fréchet and R. H. Grubbs, "A Direct Route to Cyclic Organic Nanostructures via Ring-Expansion Metathesis Polymerization of a Dendronized Macromonomer," *J. Am. Chem. Soc.*, **131**, 5388-5389 (2009).
8) Y. Xia, A. J. Boydston, Y. Yao, J. A. Kornfield, I. A. Gorodetskaya, H. W. Spiess and R. H. Grubbs, "Ring-Expansion Metathesis Polymerization: Catalyst Dependent Polymerization Profiles," *J. Am. Chem. Soc.*, **131**, 2670-2677 (2009).
9) A. J. Boydston, Y. Xia, J. A. Kornfield, I. A. Gorodetskaya, and R. H. Grubbs, "Cyclic Ruthenium-Alkylidene Catalysts for Ring-Expansion Metathesis Polymerization." *J. Am. Chem. Soc.*, **130**, 12775-12782 (2008).

6. People Working on the Project

Texas Tech
Gregory B. McKenna (Professor)
Miao Hu (Graduate Student)
Yanfei Li (Graduate Student)
Xiaoguang Peng (Graduate Student)
Stephen A. Hutcheson (Postdoctoral Researcher)
Paul A. O'Connell (Research Professor)

Caltech
Robert H. Grubbs (Professor)
Julia A. Kornfield (Professor)
Andrew J. Boydston (Postdoctoral Researcher)
Yan Xia (Graduate Student)
Christopher Daeffler (Graduate Student)
Brendan Quigley (Graduate Student)
Meisam (Iman) Hajimorad (GRA)
Rohan Hule (Postdoctoral Researcher)

7. References

[1] C.W. Bielawski, D. Benitez and R.H. Grubbs, "An 'Endless' Route to Cyclic Polymers," Science, **297**, 2041-2044 (2002).
[2] T.C.B. McLeish, "Polymers without Beginning or End," Science, **297**, 2005-2006 (2002).
[3] A.J. Boydston, Y. Xia, J.A. Kornfield, I.A. Gorodetskaya and R.H. Grubbs, "Cyclic Ruthenium-Alkylidene Catalysts for Ring-Expansion Metathesis Polymerization," J. Am. Chem. Soc., **130**, 12775-12782 (2008).
[4] Y. Xia, A.J. Boydston, Y. Yao, J.A. Kornfield, I.A. Gorodetskaya, H.W. Spiess and R.H. Grubbs, "Ring-Expansion Metathesis Polymerization: Catalyst-Dependent Polymerization Profiles," *J. Am. Chem. Soc.,* **131**, 2670-2677 (2009).
[5] P.G. Clark, E.N. Guidry, W.Y. Chan, W.E. Steinmetz and R.H. Grubbs, "Synthesis of a Molecular Charm Bracelet via Click Cyclization and Olefin Metathesis Clipping" J. Am. Chem. Soc., **132**, 3405-3412 (2010).
[6] N. Hadjichristidis, M. Pitsikalis, S. Pispas and H. Iatrou, "Polymers with Complex Architecture by Living Anionic Polymerization" *Chem. Rev.,* **101**, 3747-3792 (2001).
[7] M.W. Neiser, J. Okuda and M. Schmidt, "Polymerization of Macromonomers to Cylindrical Brushes Initiated by Organolanthanides," *Macromolecules,* **36**, 5437-5439 (2003).
[8] T.-L. Choi and R.H. Grubbs, "Controlled Living Ring-Opening-Metathesis Polymerization by a Fast-Initiating Ruthenium Catalyst," *Angew. Chem. Int. Ed.* **42**, 1743-1746 (2003); J.B. Matson and R.H. Grubbs, "Synthesis of Fluorine-18 Functionalized Nanoparticlees for use as in vivo Molecular Imaging Agents," *J. Am. Chem. Soc.,* **130**, 6731-6733.
[9] Y. Xia, J.A. Kornfield and R.H. Grubbs, "Efficient Synthesis of Narrowly Dispersed Brush Polymers via Living Ring-Opening Metathesis Polymerization of Macromonomers," *Macromolecules*, **42**, 3761-3766 (2009).
[10] Y. Xia, B.D. Olsen, J.A. Kornfield and R.H. Grubbs, "Efficient Synthesis of Narrowly Dispersed Brush Copolymers and Study of Their Assemblies: The Importance of Side Chain Arrangement" *J. Am. Chem. Soc.,* **131**, 18525-18532 (2009).
[11] A.J. Boydston, T.W. Holcombe, D.A. Unruh, J.M. J. Frechet and R.H. Grubbs, "A Direct Route to Cyclic Organic Nanostructures via Ring-Expansion Metathesis Polymerization of a Dendronized Macromonomer," J. Am. Chem. Soc., **131**, 5388-5389 (2009).
[12] J.D. Ferry, *Viscoelastic Properties of Polymers,* 3rd Edition, Wiley, New York, 1980.
[13] S.T. Milner and T.C.B. McLeish, "Parameter-free theory for stress relaxation in star polymer melts," Macromolecules, **30**, 2159–2166 (1997).
[14] E. van Ruymbeke, M. Kapnistos, D. Vlassopoulos, T.Z. Huang and D.M. Knauss, "Linear melt rheology of pom-pom polystyrenes with unentangled branches," Macromolecules, **40**, 1713–1719 (2007).
[15] R.C. Ball and T.C.B. McLeish, "Dynamic dilution and the viscosity of star polymer melts," Macromolecules, **22**,1911–1913 (1989).
[16] D.R. Daniels, T.C.B. McLeish, R. Kant, B.J. Crosby, R.N. Young, A. Pryke, J. Allgaier, D.J. Groves and R.J. Hawkins, "Linear rheology of diluted linear, star and model long chain branched polymer melts," Rheol. Acta, **40**, 403–415 (2001).
[17] M. Kapnistos, D. Vlassopoulos, J. Roovers and L.G. Leal, "Linear rheology of architecturally complex macromolecules: Comb polymers with linear backbones," Macromolecules, **38**, 7852–7862 (2005).
[18] T.C.B. McLeish, "Polymer architecture influence on rheology ," Curr. Opin. Solid State Mater. Sci., **2**, 678–682 (1997).
[19] T.C.B. McLeish, J. Allgaier, D.K. Bick, G. Bishko, P. Biswas, R. Blackwell, B. Blottiere, N. Clarke, B. Gibbs, D.J. Groves, A. Hakiki, R.K. Heenan, J.M. Johnson, R. Kant, D.J. Read and R.N. Young, "Dynamics of entangled H-polymers: Theory, rheology, and neutron-scattering," Macromolecules, **32**, 6734–6758 (1999).

[20] T.C.B. McLeish and S.T. Milner, “Entangled dynamics and melt flow of branched polymers,” Adv. Polym. Sci., **143**, 195–256 (1999).
[21] T.C.B. McLeish and R.G. Larson, “Molecular constitutive equations for a class of branched polymers: The pom-pom polymer,” J. Rheol., **42**, 81–110 (1998).
[22] S.J. Park and R.G. Larson, “Dilution exponent in the dynamic dilution theory for polymer melts,” J. Rheol., **47**, 199–211 (2003).
[23] J.H. Lee, K. Orfanou, P. Driva, H. Iatrou, N. Hadjichristidis and D.J. Lohse, “Linear and Nonlinear Rheology of Dendritic Star Polymers: Experiment,” Macromolecules, **41**, 9165–9178 (2008).
[24] Z.W. Wang, X. Chen and R.G. Larson, “Comparing tube models for predicting the linear rheology of branched polymer melts,” J. Rheol., 54, 223–260 (2010).
[25] M. van Gurp and J. Palmen, “Time-temperature superposition for polymeric blends ,” Rheol. Bull., **67**(1), 5–8 (1998).
[26] S. Trinkle, S. and C. Friedrich, “Van Gurp-Palmen-plot: a way to characterize polydispersity of linear polymers ,” Rheol. Acta, **40**, 322–328 (2001).
[27] J.R. Dorgan, J.S. Williams and D.N. Lewis, “Melt rheology of poly(lactic acid): Entanglement and chain architecture effects,” J. Rheol. 1999,43, 1141–1155.
[28] T. Inoue, K. Matsuno, H. Watanabe and Y. Nakamura, “Rheooptical study on poly(styrene macromonomer),” Macromolecules, **39**, 7601–7606 (2006).
[29] J.E. Mark, *Polymer Data Handbook,* Oxford University Press: New York: 1999.
[30] D.J. Plazek, “What’s wrong with the moduli Charley Brown: Or Get the H out and go to L,” J. Rheol., **36**, 1671–1690 (1992).
[31] D.J. Plazek and I. Echeverria, “Don't cry for me Charlie Brown, or with compliance comes comprehension,” J. Rheol., **44**, 831–841 (2000).
[32] R.G. Larson, “Combinatorial rheology of branched polymer melts ,” Macromolecules, **34**, 4556–4571 (2001).
[33] E. van Ruymbeke, C. Bailly, R. Keunings and D. Vlassopoulos, “A general methodology to predict the linear rheology of branched polymers,” Macromolecules, **39**, 6248–6259 (2006).
[34] J. Marrero and R. Gani, “Group-contribution based estimation of pure component properties,” Fluid Phase Equilibria, **183**, 183-208 (2001).
[35] Q. Jia, Q. Wang and P. Ma, “Position Group Contribution Method for the Prediction of Critical Volume of Organic Compounds,” *Journal of Chemical & Engineering Data*, **53**, 2606-2612 (2008).
[36] P.T. Mather, H.G. Jeon, A. Romo-Uribe, T.S. Haddad, and J.D. Lichtenhan, “Mechanical Relaxation and Microstructure of Poly(norbornyl-POSS) Copolymers,” Macromolecules, **32**, 1194-1203 (1999).
[37] M.L. Williams, R.F. Landel and J.D. Ferry, “The Temperature Dependence of Relaxation Mechanisms in Amorphous Polymers and Other Glass-forming Liquids,” Journal of the American Chemical Society, **77**, 3701–3707 (1955).
[38] G.B. McKenna, G. Hadziioannou, P. Lutz, G. Hild, C. Strazielle, C. Straupe, P. Rempp and A.J. Kovacs, “Dilute Solution Viscosity and Zero Shear Viscosity in the Melt of Cyclic Polystyrene Molecules,” Macromolecules, **20**, 498-512 (1987).
[39] G.B. McKenna, B.J. Hostetter, N. Hadjichristides, L.J. Fetters and D.J. Plazek, “A Study of the Linear Viscoelastic Properties of Cyclic Polystyrenes Using Creep and Recovery Measurements,” Macromolecules, **22**, 1834-1852 (1989).
[40] J. Roovers and P.M Toporowski, “Synthesis and Characterization of ring Polybutadienes,” J.Polym. Sci., Part B: Polym. Phys., **26**, 1251-1259 (1988).
[41] G.B. McKenna and D.J. Plazek, “The Viscosity of Blends of Linear and Cyclic Molecules of Similar Molecular Mass,” Polymer Comm., **27**, 304-306 (1987).

[42] K. Dodgson, D.J. Bannister and J.A. Semlyen, “Studies of cyclic and linear poly(dimethyl siloxanes). 4. Bulk viscosities,” Polymer, **21**, 663-667 (1980).
[43] M. Rubinstein, “Dynamics of Ring Polymers in the Presence of Fixed Obstacles,” Physical Review Letters, **57**, 3023-3026 (1986).
[44] Y. Ohta, Y. Kushida, Y. Matsushita and A. Takano, “SEC-MALS characterization of cyclization reaction products: Formation of knotted ring polymer,” Polymer, **50**, 1297-1299 (2009).
[45] V. Thomas, A.Y. Grosberg and K. Kremer, “Statistics of polymer rings in the melt: a numerical simulation study,” Physical Biology, **6**, 025013 (2009).
[46] S.T. Milner, T.C.B. McLeish, R.N. Young, A. Hakiki and J.M. Johnson, “Dynamic dilution, constraint-release, and star-linear blends,” Macromolecules, **31**, 9345-9353 (1998).
[47] K.L. Ngai, D.J. Plazek and V.M. O'Rourke, “Viscoelastic properties of amorphous polymers .7. Changes of the anomalous behavior of low molecular weight polystyrene with the addition of a Diluent,” Macromolecules, **30**, 5450-5456 (1997).